Dynamics of the $N(^4S_u)+NO(X\ ^2\Pi)\rightarrow N_2(X\ ^1\Sigma_g^+)+O(^3P_g)$ atmospheric reaction on the $^3A''$ ground potential energy surface. II. The effect of reagent translational, vibrational, and rotational energies

Miquel Gilibert,[a] Antonio Aguilar, Miguel González,[b] and R. Sayós
Departament de Química Física, Facultat de Química, Universitat de Barcelona, Martí i Franquès, 1, 08028, Barcelona, Spain

The effect of translational vibrational, and rotational energies on the dynamics of the $N(^4S_u)+NO(X\ ^2\Pi)\rightarrow N_2(X\ ^1\Sigma_g^+)+O(^3P_g)$ reaction has been examined using a Sorbie–Murrell analytical fitting of a grid of *ab initio* configuration interaction (CI) points for the $^3A''$ ground potential energy surface reported by the authors in a previous work. Translational energy is shown to increase total reaction cross section for all the initial rovibrational states of reactants considered. The reaction mode analysis points towards a direct mechanism and a strong influence of the shape of the potential energy surface on the reactivity, especially at low relative collision energies. Vibrational excitation of the NO reactant molecule changes the total reaction cross section values moderately, while increasing the initial rotational states of NO at low fixed relative collision energies decreases the reaction cross section sharply, eventually becoming zero for the highest J values explored. By comparing with model calculations on the same surface involving extreme $H+HL$ and $L+LH$ mass combinations, the microscopic reaction mechanism is shown to imply product molecules being created with rotational angular momentum ($\mathbf{J}'$) oriented preferentially antiparallel with respect to their orbital angular momentum ($\mathbf{l}'$) at low relative energies, with loss of orientation for higher relative energies. Thus, the surface used indicates a strong vector correlation between $\mathbf{l}'$ and $\mathbf{J}'$ and also an important influence in equipartitioning total angular momentum between the rotational and orbital angular momenta of products. Comparison with unfortunately scarce experimental data (e.g., fraction of vibrational energy in products and rate constants) shows a very good agreement.

I. INTRODUCTION

The reactions of atomic nitrogen with oxygen and nitrogen oxides are thought to play an important role in the chemistry of the upper atmosphere. In particular, the reaction
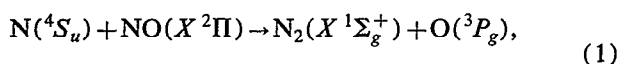
$$N(^4S_u)+NO(X\ ^2\Pi)\rightarrow N_2(X\ ^1\Sigma_g^+)+O(^3P_g),$$
(1)
$$\Delta H^0_{298}=-74.95 \text{ kcal/mol (Ref. 1)}$$

is fast enough at room temperatures for NO to be used as a titrant for nitrogen atoms,[2] or as a source of ground state oxygen atoms in discharge-flow systems.[3] This reaction is also interesting from a theoretical point of view as it proceeds with almost no activation energy and also because it can be well described at room temperature using only the ground $^3A''$ potential energy surface (PES). The importance of this system notwithstanding, very little theoretical and experimental information is available on its basic dynamical features.

The majority of the experimental measurements refer to rate constants (k) at temperatures (T) ranging from 300 to 700 K.[4-11] Recently, Michael and Lim[12] reported k measurements between 1251 and 3152 K. Their results in this temperature range are well represented by either $k=(2.34\pm0.36)\times10^{13} \exp(-113\pm260/T)$ or $k=(2.23\pm0.48)\times10^{13}$ cm³/mol s over the whole experimental range. Most of the k values obtained in these works fall within statistical error of each other and are in good agreement with the recommended value of Baulch *et al.*[13] of $(1.6\pm0.3)\times10^{13}$ cm³/mol s, independent of T. In Ref. 12, the authors suggest $(2.11\pm0.66)\times10^{13}$ cm³/mol s as a suitable value for k between 196 and 3150 K.

There seems to be a general consensus in that reaction (1) should proceed with no or very little energy barrier. This assumption has been confirmed in view of the contracted CI (CCI) calculations of Walch and Jaffe,[14] who found out an energy barrier of only 0.5 kcal/mol on the ground $^3A''$ PES connecting reactants and products. In the same paper, the authors report a 14.4 kcal/mol energy barrier for the $^3A'$ PES also correlating reactants and products in their ground electronic states, thus showing that at moderate relative collision energies, reaction (1) should be well described using the lowest $^3A''$ PES only.

The only other experimental information available about this system consists in estimates of the fraction of exothermicity going into vibration. The values given in Refs. 15 and 16 are 0.28 ± 0.07 and 0.25 ± 0.03, respectively.

In a recent work[17] (hereafter referred to as paper I), we reported preliminary quasiclassical trajectory calculations (QCT) using an analytical Sorbie–Murrell function

[a] Author for correspondence. Present address: Soreq Technology Center, P.O. Box 625, Yavne 70654, Israel.
[b] Present address: Departamento de Química, Universidad de La Rioja, Obispo Bustamante, 3, 26001, Logroño, Spain.
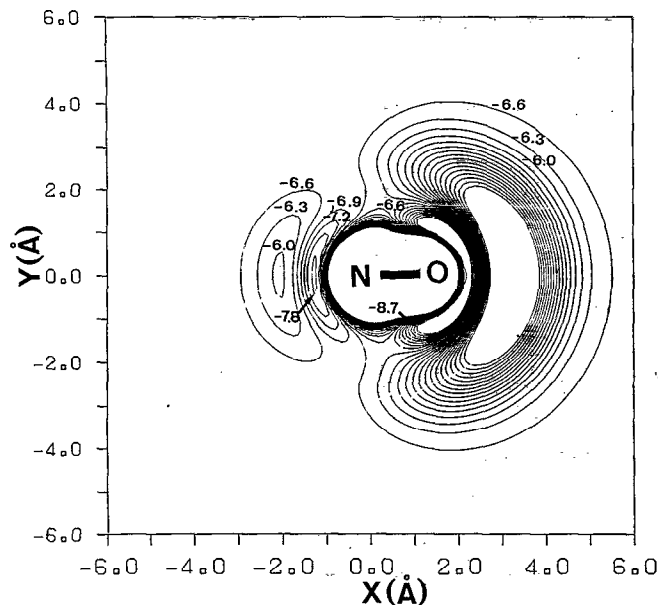
FIG. 1. Equipotential polar contour plot for the $^3A''$ Sorbie–Murrell PES with NO maintained fixed at its equilibrium bond distance with N atom at (0,0). Contours are spaced 0.3 eV with energies relative to dissociated atoms. The arrows point the lowest equipotential contours for N approaches to the N or O end of the NO molecule. The equipotential contours on the O side of the NO molecule rise in energy for a N collinear approach from the more external one placed at -6.6 eV (reactant asymptote), but those diminish for an angular N approach. More details are given elsewhere (Ref. 17).

for the $^3A''$ ground PES obtained from a fitting of a CCI grid of points[18] which enabled reproduction of the *ab initio* information with an overall standard deviation of 1.06 kcal/mol. The analytical PES showed, however, no barrier to reaction on the minimum energy path leading to products. Figure 1 displays a polar contour plot of the Sorbie–Murrell PES employed with the NO molecule kept fixed at its equilibrium bond distance. The energy rises steeply as the attack angle goes away from the saddle point value (107.1°), leaving a narrow passage for N approach to NO. When the NNO angle is varied away from the saddle point value with the NN and NO distances kept fixed at their saddle point values, the potential energy rises steeply indicating a rather repulsive behavior. The observed excitation function shape can be well interpreted[19] in terms of the angle dependent line-of-centers model (ADLOC).[20] This same model provides good fittings of the angle-dependent partial reaction cross sections at low and moderately low collision energies.

The rate constants and vibrational energy distributions in products obtained using this PES considering only the most populated rovibrational level of NO at 300 K ($v=0$, $J=7$) compare well with the experimental data. From the preliminary QCT[17,19] results, a direct reaction mode with energy being released mainly as translation of products has been inferred. As it is derived from the minimum energy reaction path, the energy decreases slightly on the path from reactants to products falling below the reactants asymptote, rising again a bit afterwards until it reaches the

saddle point geometry, subsequently experiencing a very steep descent to products. The very sudden behavior of the energy profile was invoked in paper I to account for the predominant translational excitation over the whole energy range explored.

In this work, we present the results of an extensive and complementary study on the dynamics of reaction (1) using the Sorbie–Murrell PES built up in paper I. Our goal in carrying out these calculations is to acquire a deep insight into the detailed mechanism through which this system evolves towards products, as well as to check the accuracy of the dynamical magnitudes obtained in previous references[17,19] using only preliminary QCT results. In Sec. II, a brief description of the methodology and initial conditions selected is given. Section III presents the results obtained for different dynamical properties of interest together with a discussion about them, and finally in Sec. IV some conclusions are drawn.

II. QUASICLASSICAL TRAJECTORY CALCULATIONS

QCT 3D calculations were performed on the above-mentioned PES using a QCT program developed in our laboratory[21] based on a previously existing standard version.[22] The integration methods and Monte Carlo samplings of the initial conditions were identical to those used in previous similar studies.[23–25] Trajectories were carried out for a wide range of relative translational energies [E_T =0.0388 eV (average value at 300 K) to 1.0 eV], and rovibrational states of NO ($v=0$; $J=0$, 4, 7, and 14) and ($v=1$, 2; $J=7$) to probe rotational and vibrational effects. Some additional calculations were also performed at E_T =0.0388 eV for $v=0$ and $J=1$, 2, 10, 11, 16, 25, and 36 to obtain an insight into the influence of rotation on reactivity. Besides a much more detailed grading of E_T at ($v=0$, $J=7$), the most populated rovibrational level at 300 K within the anharmonic oscillator and nonrigid rotor model was used to obtain a detailed shape of the excitation function. The results of this calculation have already been reported in paper I, but we include some of them in the present work for completeness. In all, the present study comprises about 167 000 trajectories run on the IBM 3090/600J computer of the Centre de Supercomputació de Catalunya (CESCA).

For most E_T and rovibrational conditions, an estimated number of about 1500 trajectories was enough to furnish total reaction cross section values with error estimates (one standard deviation) of less than 10% of each value. However, for the lowest relative energy value considered (E_T=0.0388 eV) to obtain a statistically significant number of trajectories to evaluate dynamical properties such as angular or vibrational distributions in products, it was necessary to increase the number of integrated trajectories to between 8000 and 10 000.

III. RESULTS AND DISCUSSION

A. Reaction mode analysis

An approximate analysis of the reaction mode has been carried out by monitoring on a graphical terminal the ev-
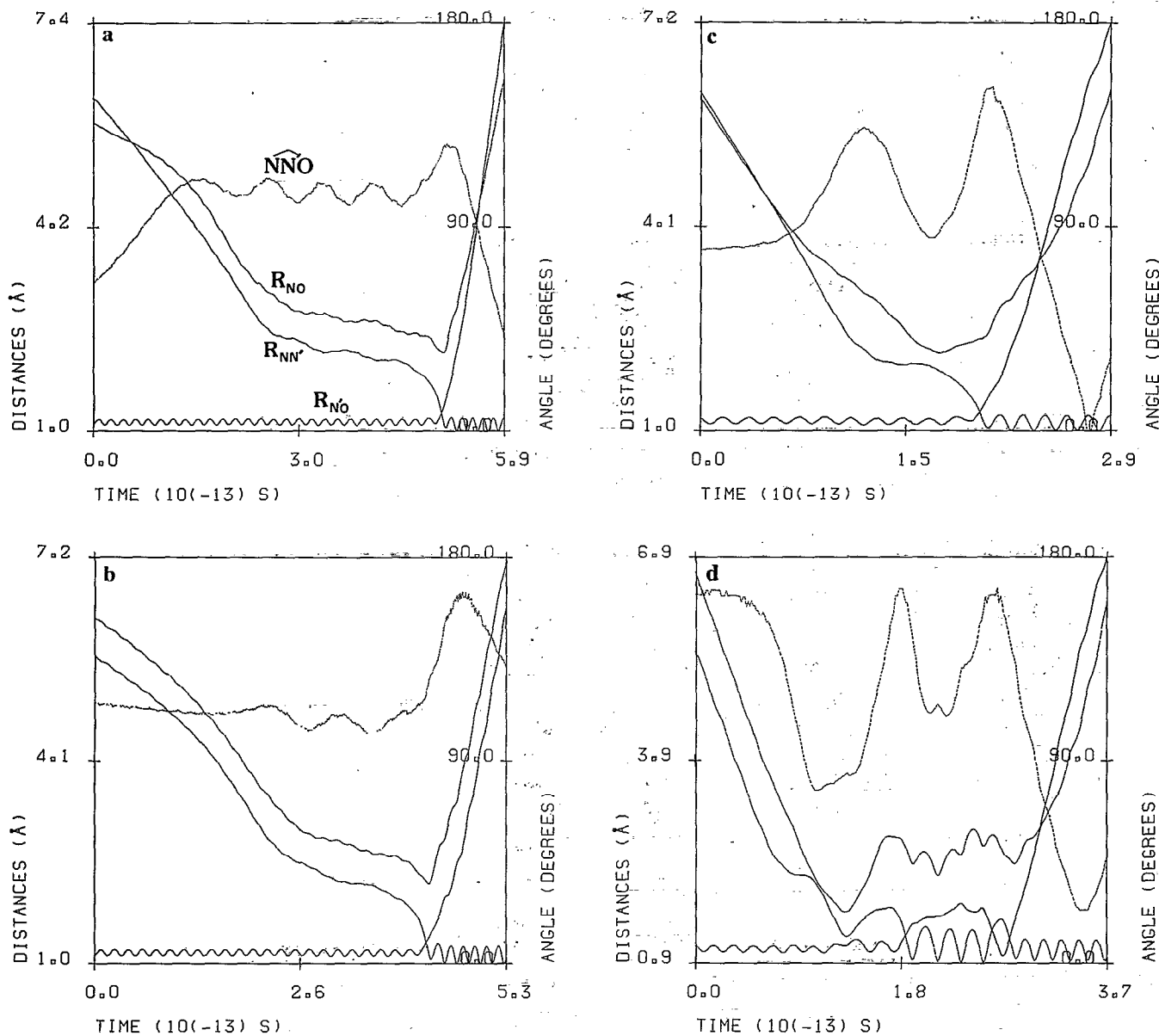
FIG. 2. Typical reactive trajectories of reaction (1) (a) E_T=0.0388 eV, v=0, and J=0; (b) E_T=0.0388 eV, v=0, and J=25; (c) E_T=0.6 eV, v=0, and J=7; (d) E_T=1.0 eV, v=0, and J=7. The continuous lines indicate the temporal evolution of the three internuclear distances and the dotted line indicates the evolution of the NNO angle.

olution of the interatomic distances of a representative sampling of trajectories at E_T=0.0388 eV with v=0 and J=0, 7, and 25, and at E_T=0.3, 0.6, and 1.0 eV, and v=0, J=7.

Figure 2 shows several plots of typical reactive trajectories for different E_T and rovibrational conditions. As was to be expected on the previous considerations about the shape of the PES, almost all reactive trajectories analyzed proceed in a direct mode. The temporal evolution of the interatomic distances evidenced that the N atom can come very close to the N end of the NO molecule (almost within the N_2 bond distance range) before the NO bond breaks. Once the N atom has come close enough to the NO molecule, the interatomic NO distance tends to grow fast-indicating that the N_2 molecule formed and the O atom are

rapidly going away from each other, in agreement with the translation excitation of products found in the preliminary calculations.[17] At the same time, the NNO angle usually peaks at values above 90° for most trajectories analyzed, indicating that configurations near that of the saddle point are being explored, in agreement to the study of the angle-dependent partial reaction cross section carried out in Ref. 19. At the higher E_T studied (1.0 eV), the reaction mode follows for some trajectories a less simplistic pattern. As can be seen in Fig. 2 (d), after the N atom has come near enough to the NO diatomic, the whole NNO system starts to vibrate along the NO and NN bonds and also through the NNO bending angle, eventually breaking to give products. For this type of trajectory, a higher degree of product vibrational excitation is observed. Thus on increasing E_T,

the forming NN bond is produced with more vibrational excitation enabling the NNO system to bounce several times between the repulsive walls of the potential before the NO bond breaks completely. However, these few collision complexes have very short lifetimes and trajectories can be mainly termed as also direct trajectories.[19]

An interesting feature of the reaction mode as evidenced in Fig. 2(b) is the behavior of the NNO angle with rotational excitation of reactants for the lowest E_T considered. Usually one would expect the NNO bond angle to explore wider ranges of values along the evolution of the trajectory as rotational excitation of the NO molecule is increased, especially at the beginning of the trajectory when the interaction with the NO molecule is still weak. However, even for the highest rotational quantum number J of NO considered, $J=25$; for those trajectories eventually leading to reaction, the NNO angle varies little and is kept constrained oscillating at values near that of the NNO saddle point angle quite early in the temporal evolution of the trajectory. The NO molecule changes thus relatively early from a free to a hindered rotation, so that the NNO system moves in such a way that the NNO angle does not vary away much from the saddle point value. Also, for most reactive trajectories studied over the whole energy range, the NNO angle distribution at the beginning of the trajectory falls not very far from the distribution recorded at a collision diameter equal to 2.5 Å, which almost overlaps the ADLOC distribution peaked at the saddle point angle,[19] effect being more evident for trajectories with low E_T. This supports our consideration that the PES exerts a very strong influence in the way reaction takes place. In a more graphical representation, we could say that the NNO angle oscillates around the minimum energy path constrained by the repulsive nature of the potential along the whole trajectory evolution which causes reorientation to occur for trajectories starting with NNO angles away from the minimum energy path value, even though this anisotropy effect is more difficult to happen as J is increased [see, e.g., Figs. 2(a) and 2(b)].

B. Excitation function and thermal rate constants

Table 1 shows the total reaction cross sections for all the main rovibrational states of the NO molecule at 300 K. Even though at energies above 0.6 eV the N(^4S_u) +NO($X\,^2\Pi$)→NO($X\,^2\Pi$)+N(^4S_u) exchange channel begins to open, its contribution to reactivity is very low. For the highest E_T condition (1.8 eV) at $v=0$, $J=7$, only 73 trajectories out of 9332 went through the exchange channel, while 2968 proceeded through N atom abstraction, so that the results for this exchange channel are not shown. The excitation function plots for selected fixed (v,J) rovibrational states are depicted in Fig. 3. For moderately low collision energies ($E_T \leq 0.6$ eV), and ADLOC excitation function dependence seems to reproduce quite well the shape of the QCT excitation function at ($v=0$, $J=7$).[19] At the higher energy values considered, the excitation function plot clearly deviates from this simple model, since some of its basic assumptions, such as that all trajectories reaching the saddle point with enough energy

in the line of centers to overcome the bending potential will eventually lead to reaction, no longer hold. In fact, it is to be expected that on increasing E_T, the number of trajectories with enough energy along the line of centers experiencing rebound will also increase, thus further disrupting one of the basic approximations made in the ADLOC model.[20,26]

Defining the average quantity $\Delta S_r / \Delta E$ to measure the contribution of the increment of relative translational, vibrational, or rotational energy (ΔE) to the enhancement of the total reaction cross section (ΔS_r), we find average values of 1.94 and 1.07 Å^2/eV for $\Delta S_r / \Delta E_v$ as the vibrational quantum number is increased from $v=0$ to $v=1$ and from $v=1$ to $v=2$ at constant E_T and J values, respectively. The effect of vibrational excitation is to cause a more modest increase in the reaction cross section than E_T. The $\Delta S_r / \Delta E_T$ for a similar rise in E_T (from 0.0388 to 0.3 eV) yields 17.08 Å^2/eV thus giving a clear demonstration of the strong influence of E_T in promoting reactivity. On the contrary, rotation causes in most cases a net decrease in S_r. Thus, the average $\Delta S_r / \Delta E_r$ at constant v and E_T for the passage from $J=0-1$ and from $J=1-2$, $J=2-4$, $J=4-7$, $J=7-10$, and $J=10-14$ are -1040.76, -236.53, -165.57, -21.17, and -13.64 Å^2/eV, respectively.

The observed behavior of the total reaction cross section S_r with the initial relative and vibrational energies of reactants corresponds well with that expected for a PES with an early saddle point[27,28] such as the one we are dealing with in this work for which vibration of reactants should contribute modestly to reactivity. In this respect, Smith[29] has pointed out that the earlier the position along the reaction path the energy barrier occupies, the less is the coupling between relative translational and vibrational motions, so that vibrational adiabaticity becomes a good approximation, but since the V–T coupling is weak, the vibronic curves are likely to run almost parallel and the shape of the PES near the saddle point changes slowly with v, so that the effects of vibrational excitation are slight. It is reasonable to suppose that in the present case, since the stretching frequency of the NNO saddle point structure is quite similar to that of the NO reactant, which could justify the moderate changes in reactivity when v goes from 1 to 2. In fact, one of the reasons for the increase in S_r with v is the slight rise in the maximum impact parameters (b_{max}) on exciting the reactants vibrationally. This increase is less apparent for high collision energies, for which there is much less dependency on the features of the surface. The slight increase in b_{max} may be explained considering that on exciting v, the region in space swept by the NO molecule is also greater. It has been shown[30] that for reactions possessing a high bending frequency at the saddle point so that the barrier to reaction increases significantly with the angle of attack, but for which the initial vibrational frequency of the reagent diatomic molecule is high and the symmetric frequency at the saddle point is low, vibration can enhance reactivity even for systems without an earlier barrier taking place under vibrational adiabaticity conditions. In the present case, however, as shown in paper I, even though the bending frequency is high (421

TABLE I. Dynamical properties for the N(^4S_u)+NO($X^2\Pi$) reaction.

v	J	$E_T{}^a$	$b_{max}{}^a$	$S_r{}^a$	f/b[b]	$E_{ac}{}^c$	$\langle f'_V \rangle^d(\delta E_{vib})^e$	$\langle f'_r \rangle^d(\delta E_{rot})^e$	$\langle f'_T \rangle^d(\delta E_T)^e$
0	0	0.0388	2.70	2.70±0.24	0.06	3.44	0.30(0.91)	0.08(0.27)	0.62(2.11)
		0.1	2.70	4.27±0.23	0.12	3.50	0.28(0.87)	0.08(0.28)	0.64(2.14)
		0.3	2.55	5.84±0.10	0.37	3.70	0.24(0.77)	0.11(0.40)	0.65(2.12)
		0.5	2.55	6.62±0.20	0.55	3.90	0.21(0.61)	0.13(0.48)	0.77(2.20)
		0.8	2.47	7.34±0.11	0.61	4.21	0.20(0.74)	0.14(0.59)	0.66(1.96)
		1.0	2.57	7.22±0.17	0.81	4.41	0.21(0.83)	0.16(0.70)	0.63(1.76)
0	1	0.0388	2.70	2.26±0.15	0.03	3.44	0.30(0.90)	0.07(0.25)	0.63(2.14)
0	2	0.0388	2.70	2.06±0.14	0.04	3.45	0.30(0.90)	0.07(0.25)	0.63(2.14)
0	4	0.0388	2.55	1.67±0.16	0.03	3.45	0.30(0.90)	0.09(0.29)	0.62(2.10)
		0.1	2.55	3.58±0.22	0.11	3.51	0.27(0.84)	0.08(0.29)	0.64(2.04)
		0.3	2.61	5.66±0.12	0.35	3.71	0.25(0.79)	0.11(0.39)	0.65(2.10)
		0.5	2.52	6.55±0.19	0.50	3.91	0.19(0.63)	0.12(0.48)	0.68(2.17)
		0.8	2.47	7.39±0.11	0.62	4.21	0.20(0.74)	0.14(0.60)	0.65(1.94)
		1.0	2.57	7.25±0.17	0.77	4.41	0.22(0.86)	0.16(0.69)	0.62(1.74)
0	7	0.0388	2.55	1.06±0.09	0.03	3.45	0.28(0.87)	0.08(0.27)	0.63(2.15)
		0.1	2.55	2.81±0.09	0.14	3.52	0.27(0.84)	0.09(0.31)	0.64(2.14)
		0.2	2.47	4.37±0.25	0.26	3.62	0.26(0.84)	0.10(0.34)	0.64(2.12)
		0.3	2.61	5.52±0.10	0.35	3.72	0.26(0.83)	0.11(0.39)	0.64(2.07)
		0.5	2.52	6.53±0.21	0.50	3.92	0.20(0.67)	0.13(0.49)	0.67(2.13)
		0.6	2.47	7.00±0.10	0.57	4.02	0.21(0.71)	0.13(0.51)	0.66(2.07)
		0.8	2.52	7.34±0.12	0.62	4.22	0.21(0.78)	0.14(0.59)	0.65(1.92)
		1.0	2.57	7.15±0.16	0.77	4.42	0.22(0.87)	0.15(0.67)	0.62(1.75)
		1.5	2.57	7.27±0.11	1.17	4.92	0.24(1.06)	0.16(0.78)	0.60(1.45)
		1.8	2.57	7.30±0.11	1.26	5.22	0.26(1.22)	0.16(0.83)	0.58(1.24)
0	10	0.0388	2.55	0.70±0.09	0.02	3.46	0.29(0.87)	0.10(0.31)	0.61(2.08)
		0.065	2.55	1.34±0.15	0.09	3.49	0.29(0.89)	0.10(0.31)	0.62(2.09)
		0.1	2.55	2.20±0.18	0.21	3.53	0.29(0.90)	0.09(0.31)	0.62(2.08)
		0.3	2.61	5.15±0.12	0.37	3.73	0.27(0.88)	0.11(0.38)	0.63(2.03)
0	10	0.5	2.52	6.38±0.18	0.53	3.93	0.23(0.77)	0.13(0.47)	0.65(2.04)
		0.8	2.61	7.38±0.11	0.67	4.23	0.22(0.82)	0.14(0.59)	0.63(1.88)
		1.0	2.57	7.08±0.16	0.81	4.43	0.23(0.90)	0.16(0.67)	0.61(1.71)
0	11	0.0388	2.55	0.72±0.09	0.03	3.47	0.31(0.95)	0.09(0.29)	0.60(2.05)
		0.0905	2.55	1.83±0.17	0.13	3.53	0.29(0.90)	0.09(0.30)	0.62(2.09)
0	14	0.0388	2.55	0.60±0.08	0.06	3.49	0.30(0.93)	0.12(0.37)	0.58(1.99)
		0.1	2.55	1.66±0.15	0.14	3.55	0.28(0.87)	0.12(0.39)	0.60(2.02)
		0.3	2.47	4.68±0.11	0.40	3.75	0.27(0.91)	0.11(0.37)	0.62(2.01)
		0.5	2.52	6.02±0.18	0.51	3.95	0.23(0.79)	0.14(0.50)	0.63(2.00)
		0.8	2.61	7.19±0.11	0.78	4.25	0.23(0.86)	0.14(0.57)	0.63(1.87)
		1.0	2.57	7.01±0.17	0.90	4.45	0.24(0.94)	0.16(0.66)	0.60(1.69)
0	16	0.0388	2.40	0.49±0.04	0.02	3.50	0.25(0.77)	0.13(0.38)	0.62(2.13)
0	25	0.0388	2.40	0.03±0.01	0.00	3.58	0.27(0.85)	0.15(0.40)	0.58(2.04)
0	36[f]	0.0388	⋯	⋯	⋯	⋯	⋯	⋯	⋯
1	7	0.0388	2.80	1.55±0.18	0.07	3.69	0.28(0.67)	0.06(0.22)	0.66(2.39)
		0.1	2.80	3.20±0.33	0.18	3.75	0.26(0.60)	0.07(0.25)	0.68(2.43)
		0.3	2.48	5.45±0.18	0.35	3.95	0.26(0.68)	0.10(0.39)	0.64(2.21)
		0.5	2.69	6.89±0.29	0.53	4.15	0.22(0.55)	0.12(0.49)	0.66(2.23)
		0.8	2.55	7.41±0.16	0.65	4.45	0.23(0.66)	0.14(0.62)	0.63(2.00)
		1.0	2.60	7.60±0.26	0.79	4.65	0.24(0.74)	0.16(0.72)	0.61(1.82)
2	7	0.0388	3.06	2.09±0.22	0.11	3.92	0.28(0.50)	0.06(0.21)	0.66(2.56)
		0.1	2.88	3.53±0.38	0.26	3.98	0.30(0.60)	0.05(0.20)	0.65(2.47)
		0.3	2.64	5.81±0.20	0.38	4.18	0.28(0.56)	0.09(0.37)	0.63(2.34)
		0.5	2.55	7.04±0.33	0.53	4.38	0.24(0.44)	0.12(0.50)	0.64(2.33)
		0.8	2.63	7.54±0.17	0.77	4.68	0.25(0.58)	0.14(0.62)	0.61(2.08)
		1.0	2.48	7.59±0.29	0.83	4.88	0.24(0.59)	0.15(0.75)	0.60(1.94)

[a]Relative translational energies (E_T) in electron volts, maximum impact parameter (b_{max}) in Ångstroms, and total reaction cross sections (S_r) in squared Ångstroms.
[b]Ratio of forward vs backward scattered trajectories in the center of mass framework.
[c]Energy (in electron volts) accessible for reaction (see the text).
[d]The fraction of accessible energy appearing as translation ($\langle f'_T \rangle$), vibration ($\langle f'_V \rangle$), and rotation ($\langle f'_r \rangle$) in products.
[e]Increments in translational, vibrational, and rotational energies when evolving from reactants to products (in electron volts) defined as in Ref. 23.
[f]No reactive trajectories found at this condition (over 8800 trajectories performed).
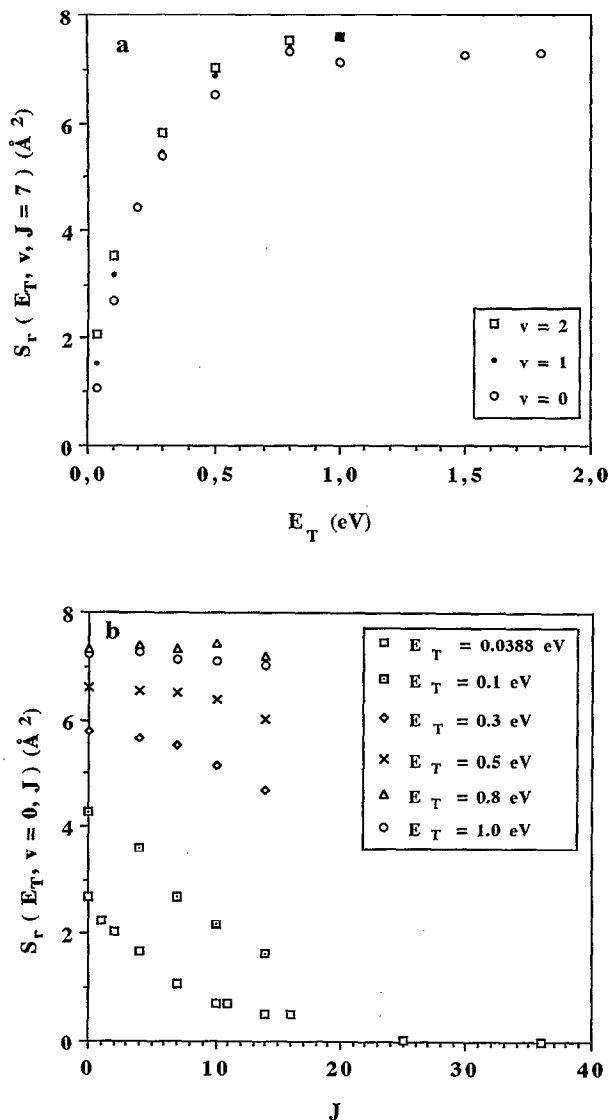
FIG. 3. Total reaction cross section plots for reaction (1). (a) Excitation function for NO at $v=0$, and 1, 2 and $J=7$; (b) evolution of the total reaction cross section with J for $E_T=0.0388$, 0.1, 0.3, 0.5, 0.8, and 1.0 eV with NO at $v=0$. Errors (one standard deviation) are indicated in Table I, but were not included here on behalf of clarity.

section with the initial J quantum rotational number of the NO reactant molecule in the ground $v=0$ vibrational level. The dramatic fall in S_r with J is more evident at low collision energies. For $E_T=0.0388$ eV, $v=0$, and $J=36$, no reactive trajectories have been found out of a total of 8800 trajectories computed. Additional calculations for $E_T=0.0388$ eV, $v=0$ at $J=50$, 100, 124, and 169 were carried out in search of an eventual rise of S_r at very high rotational energies, as has been observed in many cases.[31] Nevertheless, no reactive trajectories were found for these conditions either. A similar inhibiting behavior was observed by Persky *et al.*[32,33] in their QCT studies of the O(^3P) +HCl reaction.

At the higher energies explored, the falling behavior of the reaction cross section with J is very much attenuated [see Fig. 3(b)]. For most systems studied, the behavior of the reaction cross section with J of reactants has been explained in terms of the competing orientational and energy effects.[31,34] At low J values, the loss of the preferred orientation between the attacking atom and the diatomic molecule causes S_r to go down until it reaches a minimum value. At the same time, rotational energy may contribute to reactivity through R–V coupling. At high J values, this last effect sometimes prevails and reaction cross section rises again. In the present case, the prevailing effect at all J values considered is that of the loss of orientation. Since as we have found, vibrational motion does not contribute too much to the enhancement of reactivity, the vibration–rotation coupling expected to be found at high J values (which causes the system to behave as if having a higher degree of vibrational excitation) is not enough to counterbalance the decreasing trend motivated by the loss of orientation. Therefore, S_r continues to decrease even when the NO reagent has high rotational excitation. Consequently, for low E_T, high rotational excitations will result in the incoming N atom seeing a blurred picture of the surface as it approaches the saddle point configuration. Due to the narrow cone of acceptance around the saddle point at low E_T, most bent repulsive configurations will not lead to reaction at these energies,[17,19] so that S_r will decrease with J.

A reasonable explanation for the hindered rotation of the NNO system in trajectories with large initial J such as the one depicted in Fig. 2(b) for $v=0$, $J=25$ has been proposed in the previous subsection. From the analysis of the temporal evolution of the interatomic distances carried out at $E_T=0.0388$ eV, $v=0$, and $J=25$, we found out that only those trajectories starting with NNO angles relatively close to that of the saddle point such that the combined rotational and orbital motions of the system and the orientational effect due to the anisotropy of the potential employed, caused it to evolve around the minimum energy reaction path and led eventually towards reaction. All other trajectories starting from different angular configurations at this J did not result in reaction and were scattered back to reactants due to the repulsive nature of the potential zones explored. For higher E_T, as already stated, it is possible for trajectories starting at and evolving through more repulsive angular configurations to end up in

cm^{-1}), the stretching frequency at the NNO saddle point (1858 cm^{-1}) is similar to the vibrational frequency of NO($X\,^2\Pi$) (1904 cm^{-1}), so that actually the most important effect of increasing the initial quantum vibrational number of reactants is to induce motion in the direction of the repulsive walls of the potential, perpendicular to the coordinate leading over the barrier to products, thus not contributing very much to reactivity. From the discussion above, it follows that the relative increments in S_r with v are more important at low relative energies [Fig. 3(a)]. The less important relative enhancement of S_r with v on growing E_T is probably caused by the lesser role the detailed shape of the PES plays in determining overall reactivity at high collision energies.

Figure 3(b) shows the behavior of the reaction cross

reaction [see Fig. 2(d)], so that the effect of rotation on S_r is less apparent with growing E_T, until an almost J-independent behavior is found (see Table I). These findings are consequent with the rotating-sliding-mass model (RSMM) of Loesch[35] which predicts a strong influence of the anisotropy of the PES on the J dependence of S_r as well as a clear smoothing out of this dependence as E_T goes up.

We have also evaluated the absolute thermal rate constant $k(T)$ using fittings of the excitation function to fifth degree polynomials in E_T at different (v,J) states. For J in between values used in QCT calculations ($J=0$, 4, 7, 10, and 14), excitation functions have also been derived from estimated reaction cross sections at $v=0$ by means of a polynomial interpolation of values plot in Fig. 3(b). Then, these excitation functions have been integrated numerically by means of a standard Gaussian quadrature algorithm using the standard equation[36] and subsequently weighted according to a Maxwell–Boltzmann distribution of NO rovibrational states at each T, within the anharmonic oscillator and nonrigid rotor model, to give $k(T)$. Thus, the state specific rate constants $k(v=0, J=0\rightarrow14)$, $k(v=1, J=7)$, and $k(v=2, J=7)$ were used in these calculations, assuming that for $v=0$ and higher J values k was equal to the value for $J=14$ and that for $v=1$ and 2 all $k(v,J)$ were equal to the values for $J=7$. The last assumption is not so critical since the populations in $v=1$ and 2 are practically insignificant even at the highest temperature (at 700 K, the population in $v=0$ is of 98%). The resulting $k(T)$ values at 300, 500, and 700 K are $(1.0\pm0.2)\times10^{13}$, $(1.9\pm0.2)\times10^{13}$, and $(2.1\pm0.2)\times10^{13}$ cm^3/mol s, respectively, fall well within experimental error range [compared to experimental values of $(1.6\pm0.3)\times10^{13}$ (Ref. 13), $(2.3\pm0.9)\times10^{13}$ (Ref. 6), and $(2.9\pm1.0)\times10^{13}$ cm^3/mol s (Ref. 6)]. In general, these results improve our previous estimates of these rate constants using a polynomial fitting of the QCT excitation function for NO only at $v=0$, $J=7$ (Ref. 17) $(1.5\pm0.1\times10^{13}$, $3.0\pm0.3\times10^{13}$, and $4.9\pm0.3\times10^{13}$ cm^3/mol s, respectively) or an ADLOC fitting[19] of the same data $(0.9\times10^{13}$, 1.6×10^{13}, and 2.2×10^{13} cm^3/mol s, respectively). The agreement with the experimental magnitudes is good and the differences observed may be due to the numerical integration procedure employed (slightly different results depending on the method used) as well as to the errors introduced by the truncation of the rovibrational distribution (typically, the rovibrational states chosen for QCT calculations comprise only about 20%–17% of the total NO population in the 300–700 K range, although after the abovementioned interpolations, the limits become 84%–53%). Since as T increases, the more populated rovibrational states appear at higher J values where S_r takes lower values, the error committed in truncating at relatively low J is more evident at higher T. Our results for $k(T)$ on the $^3A''$ PES seem to support Michael and Lim's[12] considerations about this system.

C. Opacity function analysis

Figure 4 presents a plot of the opacity function at several initial E_T conditions. Recent work[19] shows that the QCT opacity and excitation functions can be well repro-
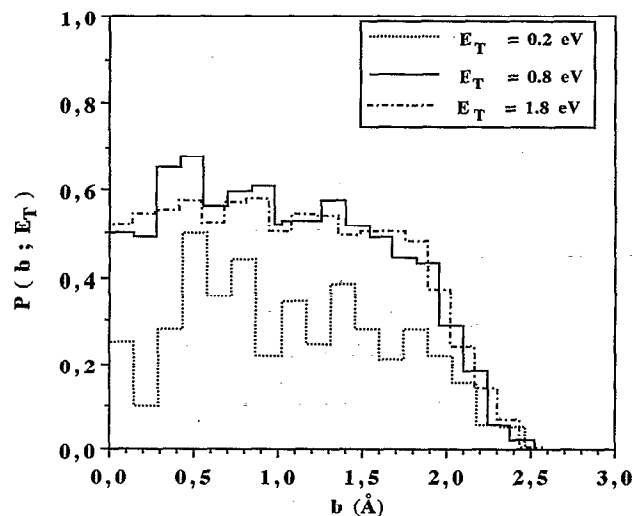

FIG. 4. Opacity function for reaction (1) at $E_T=0.2$, 0.8, and 1.8 eV and $v=0$, $J=7$.

duced assuming an ADLOC model, especially at low and moderately high E_T energies (0.0388–0.6 eV). The behavior predicted using this model shows a monotonous decrease in $P(b;E_T)$ as the impact parameter (b) approaches its maximum value leading to reaction (b_{max}), eventually becoming zero at b_{max}. Thus, $P(b;E_T)$ would exhibit its higher values at low b. As can be seen from the plots of Fig. 4, this behavior is a good approximation to the real shape of $P(b;E_T)$ over a wide range of energies. The observed depletion of $P(b;E_T)$ at low b values seems to be motivated by the poor statistics in the low b range caused by the QCT sampling scheme in which b is chosen from a uniform distribution in b^2, and the small number of reactive trajectories at low E_T energies. As has been checked,[19] if trajectories are chosen from an initial uniform distribution in b, this fall disappears and the $P(b;E_T)$ vs b plot shows a continuous decrease from $b=0$ to b_{max}. An interesting feature observed in Table I and Fig. 4 is that the b_{max} value varies little for widely differing initial rovibrational and energetic conditions. This behavior is typically found in reactions with no energy threshold, for which at the minimum energy path configuration, only the centrifugal barrier must be overcome in order for the system to proceed to products. ADLOC model predicts a constant b_{max} equal to the collision diameter (2.5–2.7 Å) regardless of the E_T value.[19]

It is also worth noting that the $P(b;E_T)$ shapes, as observed in Fig. 4, remain almost the same. Since the rotational periods of the NO molecule, assuming a rigid rotor approximation, are 2.2×10^{-12}, 1.3×10^{-12}, 9.3×10^{-13}, and 6.7×10^{-13} s for $J=4$, 7, 10, and 14, respectively, and the times inverted by the N atom in covering the 6.0 Å distance that separates it initially from the center of mass of NO would be assuming constant relative velocity of reactants, approximately 6.8×10^{-13}, 4.2×10^{-13}, 2.4×10^{-13}, 1.9×10^{-13}, and 1.3×10^{-13} s for $E_T=0.0388$, 0.1, 0.3, 0.5, and 1.0 eV, respectively, it follows that for the most of E_T and rovibrational conditions, the time it takes

for N to approach NO is shorter than the rotational period of NO. Therefore, the similar $P(b;E_T)$ shapes, almost unaffected by rotation [rotational excitation causes mainly a decrease in the area under the $P(b;E_T)$ curve as expected from the decreasing shape of the S_r vs J curve] seem to corroborate our observation that the PES is anisotropic enough to reorientate initially unfavorable NNO configurations towards more favorable dispositions (either NNO angle close to the saddle point value (107.1°) or impact parameters close to the collision diameter, which is approximately equal to the distance of the N atom to the center of mass of NO in the saddle point (2.5 Å)] for reaction to take place.

D. Energy distribution in products

The analysis of the energy distribution in products has been carried out considering the mean fraction of available energy appearing in rotation $\langle f_r' \rangle$, vibration $\langle f_v' \rangle$, and translation $\langle f_T' \rangle$ of products. For each E_T and NO rovibrational quantum level considered, the accessible energy is defined as

$$E_{ac}=E_T+E_{int}+\Delta E, \tag{2}$$

where E_{int} is the internal energy of reactants and ΔE is the exoergicity. Also the absolute quantity

$$\delta E_i=E_i'-E_i \tag{3}$$

is depicted in Table I (the primed quantities refer to products). For a given kind of energy i, this magnitude shows the variation in the energy present in that mode on passing from reactants to products.[25]

On studying the evolution of the fraction of translational energy $\langle f_T' \rangle$ and the corresponding increment δE_T, it becomes evident that for a fixed (v,J) state of NO, both $\langle f_T' \rangle$ and δE_T remain almost constant for E_T below 0.5 eV. At higher relative energies, both magnitudes decrease. For fixed values of the vibrational quantum numbers v and E_T, the rise in J does not greatly influence either the $\langle f_T' \rangle$ or δE_T obtained, even though it seems that for the higher J values considered, there is a very slight trend towards diminishing $\langle f_T' \rangle$ and δE_T. The observed effect is so low, however, that it might well stem from the statistical uncertainty in the determinations. If J and E_T are kept fixed and v is made to increase, there is a clear trend towards an augmentation of δE_T. This effect is much less evident for $\langle f_T' \rangle$, since given the large exothermicity of this reaction, most of the contribution to the accessible energy (except at high E_T) comes from the difference in the electronic energies of reagents and products, causing quantitative differences in the energy disposal of products at different conditions to be hidden when considering the fractions of energy solely.

The evolution of $\langle f_v' \rangle$ and δE_{vib} with E_T at fixed v and J as seen in Table I involves generally a slight downhill behavior until approximately $E_T=0.5$ eV, rising then again very slightly. This subsequent rise does not for many conditions bring $\langle f_v' \rangle$ above the value it had at the lowest collision energies (see, however, that for $v=2$, $J=7$, a

rather oscillating behavior for $\langle f_v' \rangle$ and δE_{vib} is observed). No clear conclusion can be drawn on the behavior of $\langle f_v' \rangle$ and δE_{vib} when the initial quantum rotational number of reactants J is increased for fixed E_T and v values. As in the case of translation, the effect is so slight that any deduced trend may be due simply to the statistical uncertainty. However, on varying v of NO from 0 to 1 and 2 with E_T and J kept fixed, a clear decrease in δE_{vib} is observed at all energetic conditions, even though the corresponding $\langle f_v' \rangle$ do not change significantly for the reasons given above.

Finally, mention should be made of the behavior of $\langle f_r' \rangle$ and δE_{rot} over the different E_T and rovibrational levels explored. The most important and clear trend found in the product energy distribution for this system is the monotonous increase in $\langle f_r' \rangle$ and δE_{rot} for fixed values of v and J as E_T is increased. For certain rovibrational levels (cf. $v=0$ and $J=0$, 4, and 7), $\langle f_r' \rangle$ almost duplicates over the whole energy range explored and, at the same time, the corresponding δE_{rot} may be two to three times greater at the higher E_T with respect to the lowest E_T explored. Again, no clear influence of the initial J on the $\langle f_r' \rangle$ and δE_{rot} values at fixed E_T and v can be deduced after inspection of Table I. The differences observed might be very well due once again to statistical deviations. The behavior with rising v at fixed E_T and J is somewhat different. For $E_T \leqslant 0.5$ eV, both $\langle f_r' \rangle$ and δE_{rot} tend to diminish with growing v, while for higher E_T, this trend inverts and both magnitudes tend to increase with rising vibrational excitation of reactants.

To attempt an explanation for the features of the energy distribution, we must first take into account that most trajectories, as seen in a previous section, proceed through an almost pure direct mechanism. Second, as noted before, the b_{max} values at the different energetic and rovibrational conditions considered are relatively low and their value does not practically change over the whole E_T range explored. It might also be illuminating to consider the E_{ac} at each (E_T,vJ) condition used in QCT calculations. From the data in Table I, it can be seen that, except for the higher E_T considered, the contribution of relative and internal energies of reactants to the total accessible energy is small compared to the amount of energy coming from the difference in electronic energies between the ground states of the NO and N_2 molecules (3.29 eV), so that the fall from reactants to products will always play an important role in determining the reaction mechanism over a wide range of energies, implying also as stated above only small variations in the energy fractions. Finally, the bent nature of the saddle point on this PES (107.1°) would tend to favor accessible energy being channeled to rotation of products.[27] Thus, when E_T rises, δE_{rot} does as well grow.

As advanced in paper I, the main energetic effects observed stem primarily from the high exothermicity and marked anisotropy of the PES of the system. At low E_T, the sharp decrease in energy observed after the saddle point and the direct character of the trajectories cause energy to be released primarily as repulsion in the NO direction resulting in translational motion of products. On in-

creasing E_T a little, the NNO angular scope around the saddle point configuration leading to reaction widens a bit, contributing to rising slightly $\langle f'_r \rangle$ and δE_{rot} (because of the combined effects of the bent saddle point and the possibility that more bent configurations away from the minimum reaction energy path may become reactive), while leaving the product translational energy contents almost unchanged {since more E_T results, at most, in a faster motion of N relative to NO after the saddle point [see Figs. 2(c) and 2(d)]} and making $\langle f'_v \rangle$ and δE_{vib} decrease very slightly. In that paper, we indicated that on increasing E_T enough, the scope of NNO angular configurations eventually resulting in reaction expands considerably, with open ones tending to give N_2 product molecules in excited v' states {since in this case, the NN bond is compressed while forming [see Fig. 2(d)]} and with bent ones favoring low v' values. Hence, increasing the E_T contents contributes to populating both the low and high v' levels in products, implying only moderate increases in $\langle f'_v \rangle$ and δE_{vib} [and a more statistically resembling $P(v')$ distribution (see below)] and also to a higher rotational excitation of products (since bent NNO configurations usually result in O exerting a torque on N_2 and this latter going away tumbling), all at the expense of the translational energy contents of products. As seen in Table I both these effects make that, at $E_T \geqslant 1.0$ eV, the sum $\delta E_{\mathrm{vib}} + \delta E_{\mathrm{rot}}$ almost overcomes δE_T, thus reflecting a change in the way ΔE is distributed among products. It is also worth noting that, on increasing E_T, the shape of the surface loses importance in establishing the outcome of trajectories, so that the energetic contents and energy distributions of products should become more similar to the statistical limits. On the other hand, the strong dependence of the reactivity on the NNO configuration at the saddle point could explain the small differences encountered in the energy distributions when changing the initial rovibrational state of reactants.

The results of Figs. 5(a) and 5(b) correspond to typical translational energy distributions for the products of reaction (1). Error bars have been omitted for clarity. The data in this figure indicate that the initial vibrational state of reactants does not greatly influence those distributions. Similar plots for fixed E_T and v (not shown in Fig. 5) indicate that the initial rotational quantum number of reagents does not influence the shape of the energy distribution either. All QCT distributions exhibit important fractions of the N_2 population at relatively high E'_T in accordance with the observed translational excitation of products. Almost no molecules are obtained with E'_T below 1.0 eV, the distribution being slightly broader for $E_T = 1.0$ eV in accordance with the slightly wider rotational and vibrational energy distributions observed at this energy. The shape of both curves does not obviously conform to a typical Boltzmannian curve, not showing any clear maxima (the observed spikes are more probably due to the binning of E'_T than to real dynamically induced structures) and behaving instead relatively even between 1.5 and 4.0 eV. This shows that even though the N_2 molecules are mostly produced with high relative energy, the final contents vary very much according to the evolution of the
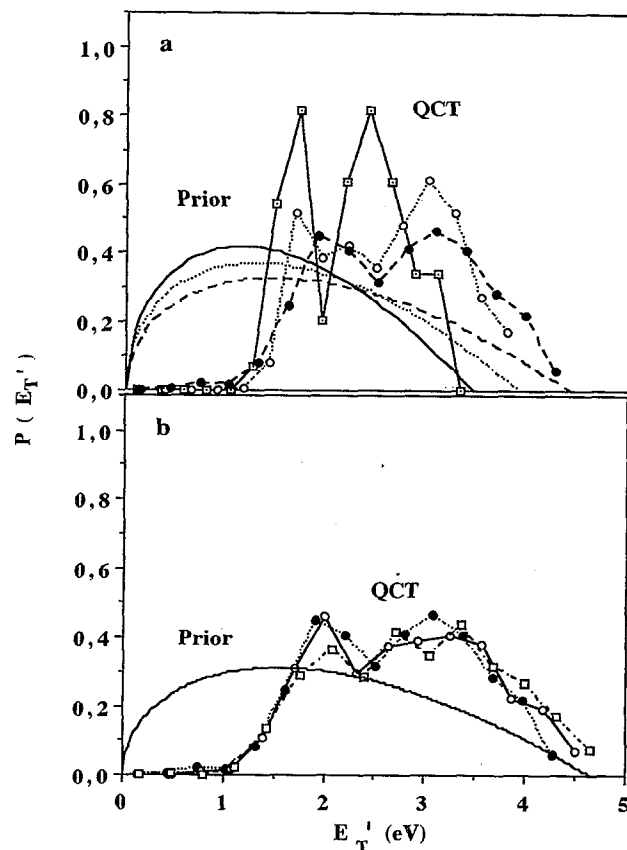

FIG. 5. QCT and prior translational distributions for reaction (1) at several conditions (a) $v=0$, $J=7$; $E_T=0.0388$ (solid line), 0.5 (dotted line), and 1.0 eV (dashed line). (b) $J=7$, $E_T=1.0$ eV; $v=0$ (dotted line), 1 (solid line), and 2 (dashed line). Lines with points are used for QCT distributions and without points for the corresponding prior distributions.

system in its passage to products. Also, superimposed on Fig. 5(a), plots of the corresponding prior distributions for E'_T following the vibrating rotor model (VR) of Levine *et al.*[28] are presented for comparison with the QCT data. According to this scheme, the expected probability distribution for the relative translational energy of products at a certain E_T is given by

$$P^0(E'_T) = \frac{E'^{1/2}_T \sum_{v'=0}^{v'^*}(1/B_{v'})}{\sum_{v'=0}^{v'^*}\sum_{J'=0}^{J'^*(v')}(2J'+1)(E_{\mathrm{ac}}-E_{v'J'})^{1/2}} \quad (4)$$

with $B_{v'}$ the rotational constant corresponding to the vibrational level v' of products, $E_{v'J'}$ the rovibrational energy of products within the VR scheme, and v'^* and $J'^*(v')$ the maximum values of the vibrational and rotational quantum numbers of products satisfying $E_{v'J'} \leqslant E_{\mathrm{ac}}$. The prior distributions obtained in this manner do almost superimpose on those derived using the simpler rigid rotor and harmonic oscillator (RRHO) approximation, for which the maxima in $P^0(E'_T)$ fall always at $E'_T = E_{\mathrm{ac}}/3$.

As can be seen in Figs. 5(a) and 5(b), the QCT $P(E'_T)$ distributions are peaked at higher translational energies than the prior statistical ones for all conditions explored. The prior distribution maxima fall at $E'_T = 1.15$,
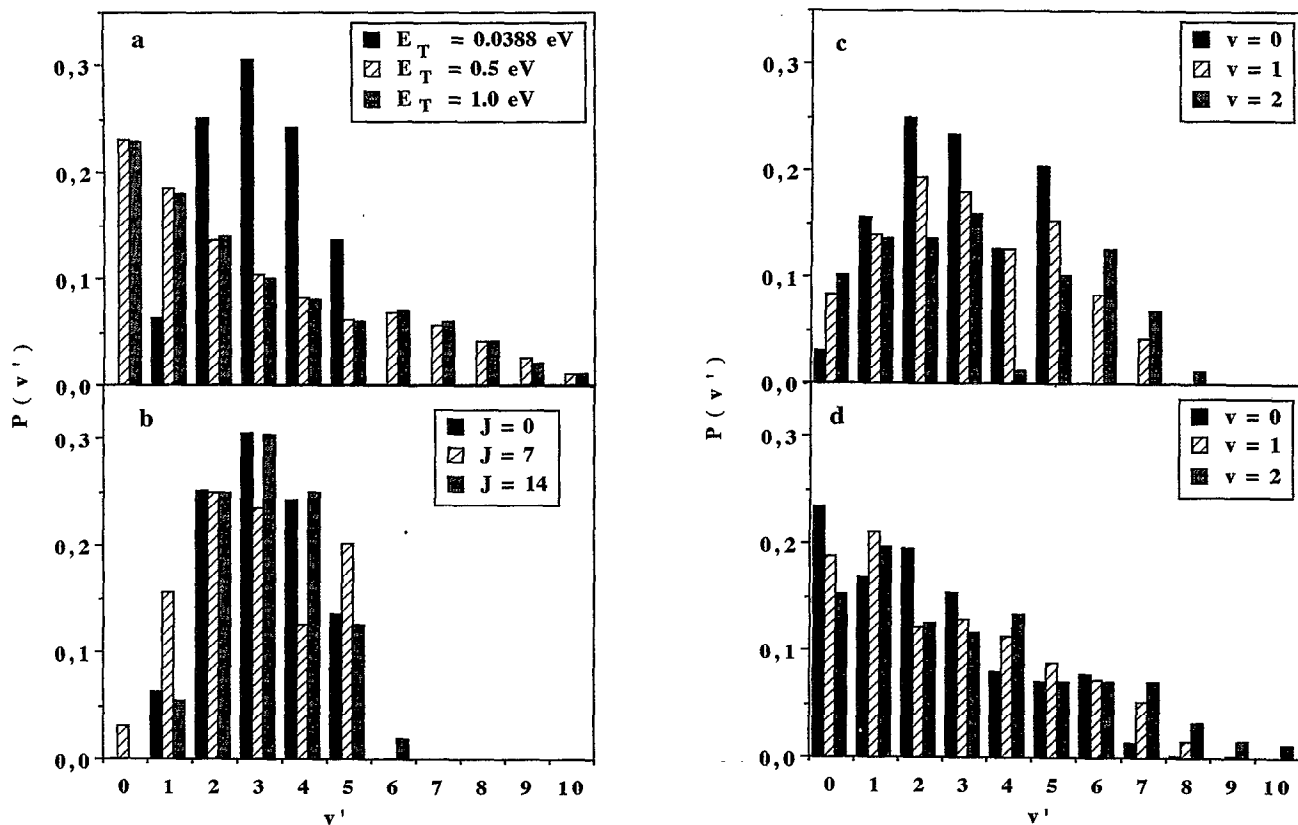
FIG. 6. QCT vibrational distribution of the N_2 product for reaction (1) at several E_T and NO rovibrational states: (a) $v=0$, $J=0$; $E_T=0.0388$, 0.5, and 1.0 eV. (b) $v=0$, $J=0$, 7, and 14; $E_T=0.0388$ eV. (c) $v=0$, 1, 2, and $J=7$; $E_T=0.0388$ eV. (d) $v=0$, 1, 2, and $J=7$; $E_T=0.5$ eV.

1.31, and 1.47 eV for $E_T=0.0388$, 0.5, and 1.0 eV, respectively, with $v=0$ and $J=7$ [Fig. 5(a)], and at $E'_T=1.55$ for $E_T=1.0$ eV with $v=1$ and $J=7$ [Fig. 5(b)]. These facts are reflected in the average $\langle f'_T \rangle$ which for the prior distributions fall around 0.43, about 20% lower than the usual magnitude derived from QCT calculations (0.58–0.68). The essentially nonstatistical behavior of the translational energy release in products is maintained over a wide range of initial translational energies and NO vibrational levels, as evidenced by the plots of Fig. 5. Only the prior distribution for the $v=1$, $J=7$ condition is shown in Fig. 5(b) on behalf of legibility, since all three prior distributions almost overlap each other, but for a short energy range. Similarly as in the $v=0$ case, the QCT distributions for $v=1$ and 2 are rather hotter than the prior ones.

Some typical quantum vibrational distributions in products obtained by means of a quantization of the classical rovibrational energy of the N_2 molecule following the method proposed by Muckerman[37,38] are presented in Fig. 6. Other methods based on action-angle variables could be more reliable for quantization of higher rovibrational levels[39] of product or reactant molecules. Figure 6(a) depicts the behavior of the vibrational quantum distribution in products $P(v')$ with the relative energy of reactants. It can be seen that at the lowest translational energy explored, a vibrational inversion peaked at $v'=3$ is found. This situation continues for higher E_T values, up to 0.3 eV, but is not found at $E_T \geqslant 0.5$ eV, where a smoothly decreasing distri-

bution is observed. As can be seen in Fig. 6(b), the initial J state of the NO reactant molecule does not alter substantially the general features of $P(v')$. The very rough trend observed for all relative energies explored seems to be for J to increase the number of populated levels as J goes up, but never altering enough the shape of the $P(v')$ distribution at high E_T so as to achieve a vibrational inversion situation as the one observed for low E_T. The effect of vibrational excitation of reactants is similar to rotation [see Figs. 6(c) and 6(d)]. In this case though, it causes a $P(v')$ inversion to arise at $v'=1$ for $E_T=0.5$ eV, when v goes from 0 to 1 or 2 [Fig. 6(d)].

As in the case of the translational energy distribution, to check the way vibrational energy is distributed into products, we have calculated as well the prior vibrational distribution within the VR model following the scheme of Levine *et al.*[40,41] to be compared with the QCT results. The expected probability distribution of levels v' at a certain E_T is given in general by

$$P^0(v') = \frac{\sum_{J'=0}^{J'^*(v')} (2J'+1)(E_{ac}-E_{v'J'})^{1/2}}{\sum_{v'=0}^{v'^*}\sum_{J'=0}^{J'^*(v')}(2J'+1)(E_{ac}-E_{v'J'})^{1/2}} \quad (5)$$

with $E_{v'J'}$ expressed according to the VR model.

Figure 7 plots the prior and QCT distributions for $E_T = 0.0388$ and 1.0 eV and NO at $v=0$, $J=7$. Obviously, the observed behavior even though there is considerable statistical error, deviates greatly from the statistical expectations
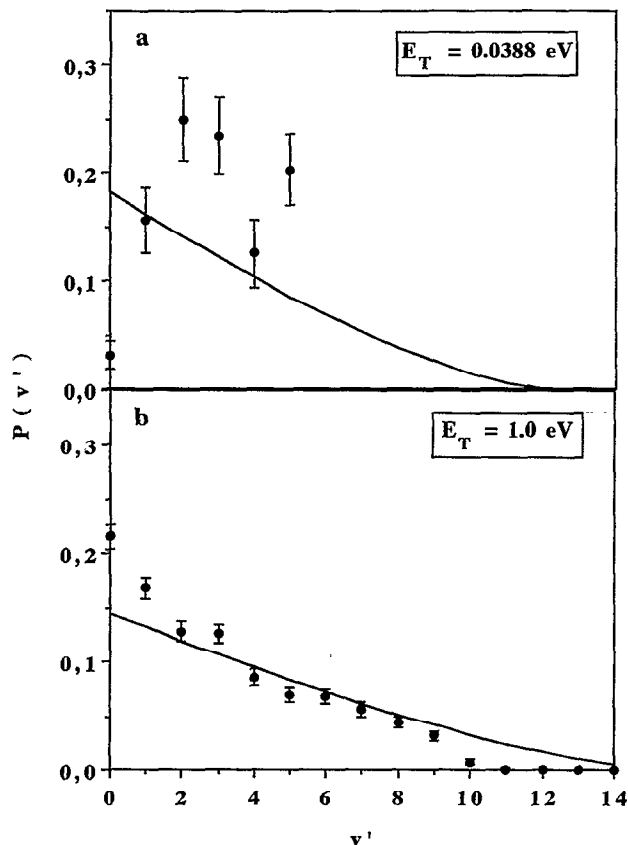
FIG. 7. QCT and prior vibrational distributions for reaction (1) at several conditions: (a) $v=0$, $J=7$; $E_T=0.0388$ eV and (b) $v=0$, $J=7$; $E_T=1.0$ eV. The solid line shows prior vibrational distribution.

FIG. 8. QCT and prior rotational distributions of reaction (1) at $v=0$, $J=7$, and $E_T=0.5$ eV (solid line) and 1.0 eV (dashed line) for different vibrational levels of the N_2 product molecule (a) $v'=0$ and (b) $v'=1$. Lines with points are used for QCT distributions and without points for the corresponding prior distributions. Both kind of distributions are normalized to area unity.

at 0.0388 eV, while both plots are similar at 1.0 eV. The strong nonstatistical nature of the N_2 vibrational population produced in reaction (1) is maintained up to relatively high E_T (in some cases even for 0.5 eV) for many initial rovibrational conditions examined in the present work. An attempt at obtaining information about the constraints to vibrational energy partitioning by performing a surprisal analysis yielded no clear behavior of the surprisal plot for the lower energies. However, at high and moderately high E_T energies (0.8 eV and above), the surprisal approaches a straight line. The QCT $P(v')$ distribution at high E_T tends to fall more steeply than the prior one [Fig. 7(b)] being more peaked towards low v' than the statistical expectation. This fact implies that the QCT vibrational distribution is in general somewhat cooler than the prior one. The $\langle f'_V \rangle$ values corresponding to the prior distributions are 0.26 (at $v=0$, $J=7$, and $E_T=0.0388$ eV) and 0.27 (at $v=0$, $J=7$, and $E_T=1.0$ eV), while the analogous QCT values are 0.28 and 0.22, respectively, in general somewhat lower. Experimental values of $\langle f'_V \rangle$ at 300 K are within the 0.25–0.28 range,[15,16] quite close either prior or to the QCT value at the lowest E_T.

The change in the behavior of $P(v')$ with E_T arises probably from the decreasing influence of the shape of the potential in determining the mechanism of reaction (1); at low collision energies, the repulsive shape of the PES and the bent nature of the saddle point as well as the sudden
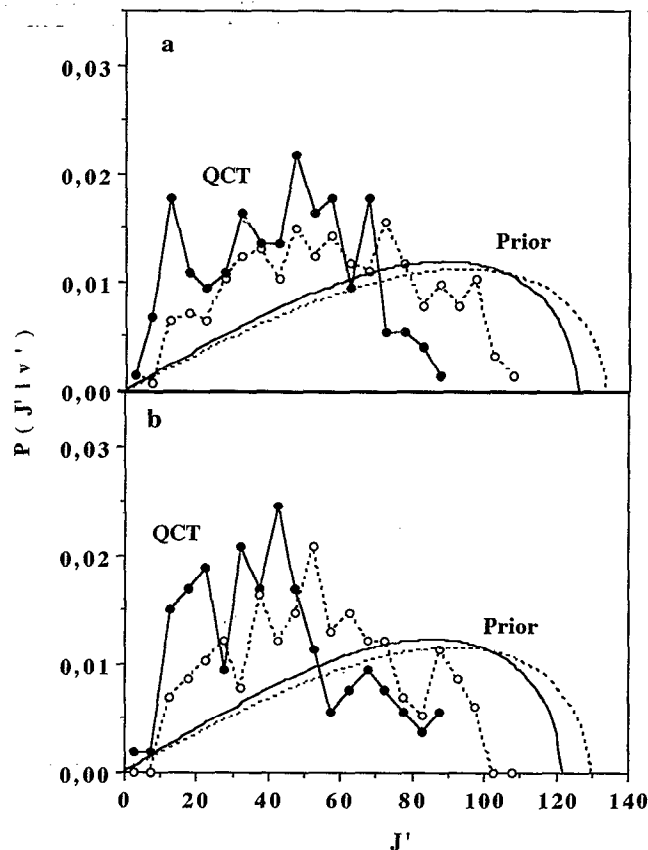
and direct mechanism for energy release in products prevent vibrational energy to be disposed of statistically, favoring vibrational inversion and also limiting the number of product quantum states accessible. In fact, as stated in paper I, on monitoring the v' values for trajectories evolving with NNO angles near the saddle point one, we observe a vibrational inversion at about $v'=2$. As E_T reaches higher values, the reaction mode is less dependent on the shape of the PES, and besides, the NNO structure can explore a wider range of configurations, and may also channel vibration towards its bending and stretching modes [see Fig. 2(d)] favoring a more statistical energy partitioning in products (with more N_2 molecules produced in $v'=0$, but also in $v'=4$). With that, a seemingly more statistical vibrational distribution corresponding to little constrained v' distribution becomes more likely as can be seen in Fig. 7(b) for $E_T=1.0$ eV (see paper I).

In Fig. 8 we present the distribution of the population of N_2 rotational levels at different vibrational levels for several initial rovibrational and energetic conditions. No conclusions ought to be taken from the detailed oscillating shapes of these QCT distributions due to the large error bars, which were not shown only on behalf of legibility. Due to the small number of trajectories obtained at low E_T

the distributions we give correspond to energetic conditions for which splitting the different v' levels of products in terms of rotational quantum levels J' makes statistically speaking sense. As for the plots showed, the distributions have been built by ordering the rotational population of each v' in bins of five J' due to the closeness of the N_2 rotational levels and renormalizing to unity. The corresponding prior $P^0(J'|v')$ vs J' curves were obtained according to the standard formula

$$P^0(J'|v') = \frac{(2J'+1)(E_{ac}-E_{v'J'})^{1/2}}{\Sigma_{J'=0}^{J'^*(v')}(2J'+1)(E_{ac}-E_{v'J'})^{1/2}} \quad (6)$$

with $E_{v'J'}$ expressed according to the VR approximation as stated above. These distributions are also shown superimposed on Figs. 8(a) and 8(b). The prior rotational distributions as well as those coming from QCT calculations are normalized to unity, so that the areas under the curves do not reflect the relative populations of the corresponding v' levels.

For all v' levels, we observe QCT broad bell-shaped distributions peaked at approximately the same J' interval. As E_T goes up, the range of attainable J' levels grows [see Figs. 8(a) and 8(b)] and the maxima of the $P(J'|v')$ distributions shift to higher J', indicating the augmentation in the overall rotational energy contents of the product molecules as initial relative energy is raised. Care must be taken when drawing conclusions about the QCT distributions, however, since they still bear relatively high statistical errors. The statistics are too modest for a $P(J'|v')$ plot at $E_T=0.0388$ eV (average thermal energy at 300 K) to be of interpretative value, but it seems reasonable to suppose in view of the general behavior of this system that the QCT $P(J'|v')$ plot at this energy will not greatly differ in shape and behavior from the ones given in Fig. 8.

Even though these bell-shaped distributions clearly do not correspond to thermal distributions at 300 K since most N_2 molecules are produced with relatively high J' values, they do not either conform to the statistically expected ones. On the contrary, they are notably cooler than the prior distributions, since the maxima for these latter usually appear at J' zones for which the QCT results do not yield large N_2 populations (see Fig. 8). However, on growing E_T there seems to be a slight trend towards populating the higher J' levels more [the QCT $P(v'|J')$ curves enlarge more in the high J' branch with E_T] as expected from the considerations made above. Also the QCT populations at low and high J' levels are not negligible due to the broad form of the $P(J'|v')$ curves, indicating that N_2 molecules are produced with rather variable rotational energy contents. The combined compensating effect of the hot $P(E'_T)$ and cold $P(J'|v')$ QCT distributions when compared to the corresponding prior ones could explain why the $P(v')$ QCT distribution resembles the prior one at sufficiently high E_T. Unfortunately, no experimental data exist on either rotational or translational energy distributions to be compared with. Experimental work on both aspects would be desirable to assess the validity of the present theoretical results.
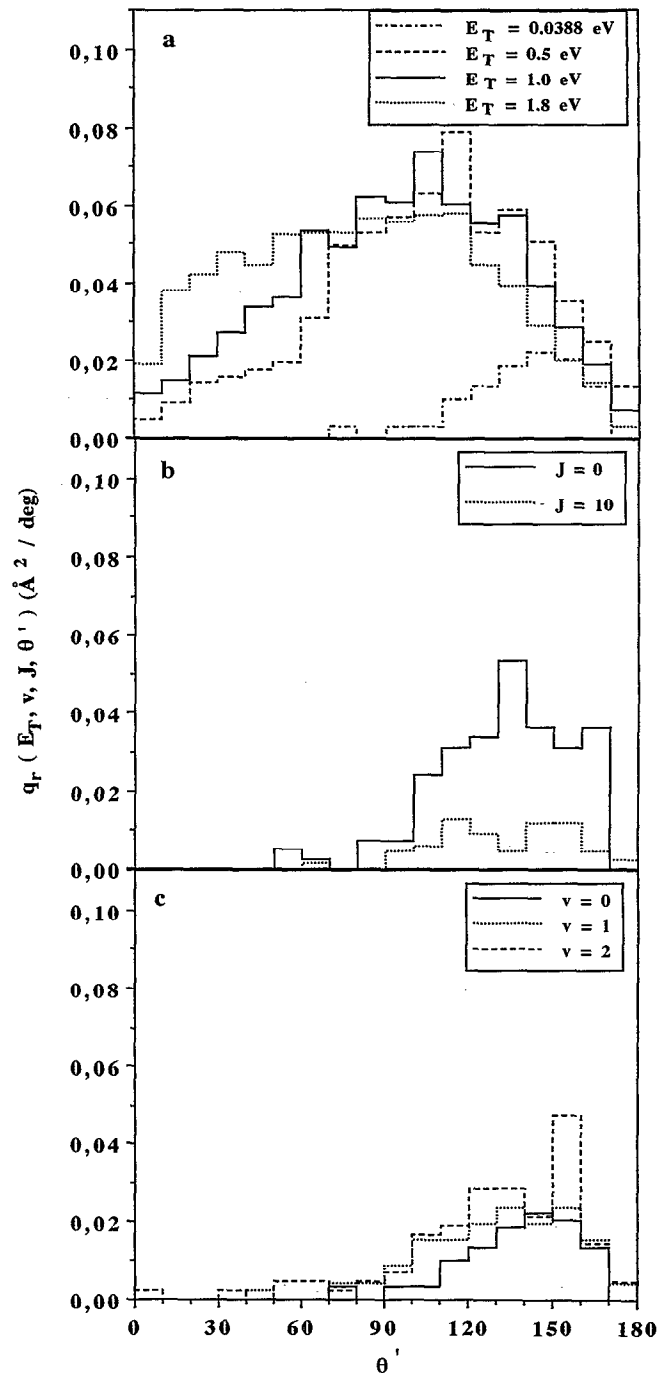

FIG. 9. Polar differential reaction cross section at several initial conditions: (a) $v=0$, $J=7$; $E_T=0.0388$, 0.5, 1.0, and 1.8 eV; (b) $v=0$, $J=0$ and 10; $E_T=0.0388$ eV; (c) $v=0$, 1, 2, and $J=7$; $E_T=0.0388$ eV.

E. Angular distribution in products

The angular distribution study of the N_2 molecules produced in the center of mass framework has been undertaken using the standard polar differential reaction cross section $q_r(E_T,v,J;\theta')$,[42] where reactive trajectories were binned in intervals of ten degrees in the angle of scattering (θ'). This property enables a more detailed examination of

the forward/backward (f/b) scattering ratio and total re-action cross section, which are depicted in Table I for all conditions studied.

Typical results for q_r are plotted in Fig. 9 for different rovibrational and E_T conditions. Once again, no correlation is found between the initial rovibrational state of reactants and the final f/b ratio of reaction (1). On the other hand, on increasing translational energy, the f/b ratio increases also significantly leading to more forward scattering. It is thus that at the highest E_T for which QCTs have been calculated (1.8 eV), the reaction acquires a considerably forward character. The predominantly backward scattering found for most relative energy conditions is consequent with the direct mechanism outlined before, involving repulsive energy release along the NN bond[27,28] also encountered in other systems with direct trajectories.[24] Since b_{max} remains almost constant over the whole E_T, it seems that trajectories at high and low E_T proceed in a similar manner (as seen in a previous section, the overall shape of the opacity function is approximately the same irrespective of initial energy). The relatively low values found for b_{max} point towards a direct mechanism in which the repulsion induced by the close vicinity of N to NO expel the N_2 product molecule backwards in the center of mass framework, overcoming the trend of the forming N_2 product to continue forward in the center of mass system. However, at higher collision energies, the higher velocity of the incoming N atom together with the accelerating effect of the downhill potential after the saddle point are enough to overcome the repulsion between the N_2 molecule formed and the outgoing O atom and force the N_2 product to continue forward in the center of mass framework. Thus, trajectories would be produced in forward angles mainly because of the inertial effect of the incoming N atom. This mechanism depending only on the relative energy of the motion of the N atom, the proportion of forward vs backward scattered NO molecules will not rely significantly on the amount of vibrational or rotational excitation of reactants as observed from Table I and Figs. 9(b) and 9(c).

F. Angular momentum disposal in products

In a general $A + BC$ scattering experiment, the product distribution has three angular degrees of freedom, usually taken as the θ' scattering angle between the incoming **k** and outgoing **k'** relative velocities (cf. the previous subsection), the orientation angle χ between **k** and the rotational angular momentum **J'** of products (the bold quantities represent vectors), and the dihedral angle ϕ between the **kk'** and **kJ'** planes. The differential cross sections for each one of these angles may be defined in terms of the associated Legendre polynomial series.[43,44] Scalar parameters defined as

$$\Lambda = \left\langle \frac{l}{(l+J)} \right\rangle, \quad \Lambda' = \left\langle \frac{l'}{(l'+J')} \right\rangle, \qquad (7)$$

where l and J refer to the moduli of the orbital and rotational angular momenta of reactives or products (primed magnitudes)[45,46] can be useful to describe two vector cor-

TABLE II. Average macroscopic indicator of vector correlation for reactives (Λ) and products (Λ') of reaction (1) at several initial rovibrational and E_T conditions. The results for model mass combinations $H+HL$ and $L+LH$ are indicated by HHL and LLH.

E_T	v	J	Λ	Λ'
0.0388	0	1	0.91±0.05	0.54±0.14
0.0388	0	4	0.77±0.09	0.52±0.15
0.0388	0	7	0.66±0.11	0.49±0.16
0.5	0	4	0.92±0.06	0.55±0.18
0.5	0	7	0.88±0.07	0.55±0.19
0.5	1	7	0.88±0.07	0.54±0.19
0.5	2	7	0.88±0.07	0.53±0.18
1.0	0	7	0.91±0.07	0.57±0.18
0.5 (*HHL*)	0	17	0.87±0.08	0.35±0.18
0.5 (*LLH*)	0	17	0.80±0.09	0.65±0.17

relations, although logically detailed correlation of those vectors quantities is often more instructive. For typical reactions in which $l \gg J$ in the entrance channel $\Lambda \rightarrow 1$. This is the situation for many of the initial rovibrational and energetic conditions considered in this study (see Table II).

For situations in which $l' \ll J'$, $\Lambda' \rightarrow 0$, and, conversely, for cases corresponding to $l' \gg J'$, an obvious $\Lambda' \rightarrow l$ is found. Many of these limiting constraints to angular momentum disposal occur because of the mass combinations of the system. As already mentioned before, in the particular case of reaction (1), the relatively similar reduced masses of reactives and products is not likely to impose any very relevant kinematic constraint upon the angular momentum distribution in products. However, as it can be seen in Table II, the average Λ' values resemble each other very much for a wide variety of initial conditions, usually falling near 0.5–0.6. The Λ' indicator for the hypothetic mass combinations $H+HL$ and $L+LH$ on the $^3A''$ PES (with H and L having masses of 127 and 14 amu, respectively) is also shown. It seems that for most conditions the system approaches a little bit more the $L+LH$ case rather than the $H+HL$ situation, i.e., that angular momentum is somewhat more effectively being transferred to orbital angular momentum than to rotational angular momentum of products. To obtain a deeper insight of this effect, we have plotted the l' and J' moduli as a function of the module of the initial orbital angular momentum of reactives l. These plots have shown that there was a considerable concentration of points near the $l'=l$ line [see Fig. 10(a)], similarly as was found for the $L+LH$ model system [Fig. 10(c)], while not resembling the HHL case as evidenced in the plot of Fig. 10(b) indicating a clear correlation between both vectors. On representing the probability distribution for J' and l' over the whole energy range explored, no great difference between the l' and J' moduli distribution is found (Fig. 11), albeit the latter tends to peak at lower values, while the l' distribution spans a wider angular range and peaks at higher values, justifying the Λ' values observed.

We have also examined the way in which both orbital and rotational angular momenta of products are produced. To do this, we have plotted the probability distribution for the $J'l'$ and χ angles. *For all conditions explored, the* χ
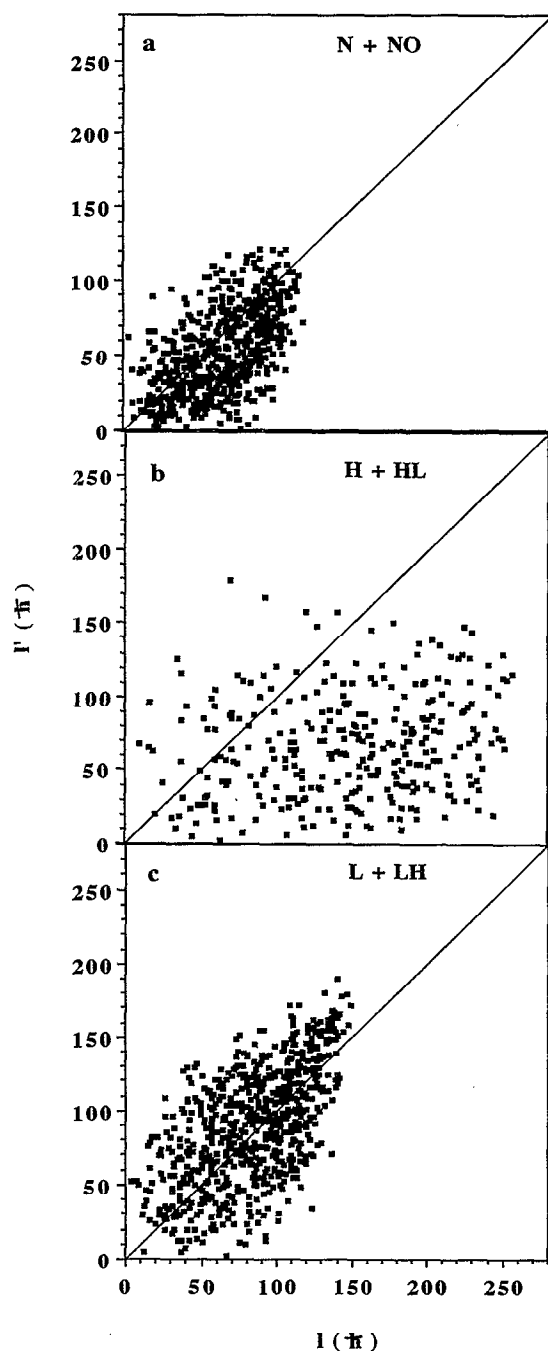
FIG. 10. Correlations between the orbital angular momenta of reactants and products: (a) plot of l' vs l for reaction (1) with $v=0$, $J=7$; $E_T=0.5$ eV; (b) model $H+HL$ mass combination with $v=0$, $J=17$; $E_T=0.5$ eV; (c) model $L+LH$ mass combination with $v=0$, $J=17$; $E_T=0.5$ eV.

angle shows a considerable broad distribution centered at 90°, very similar to the one observed for the $L+LH$ model system. The behavior of the $\mathbf{J}'\mathbf{l}'$ angle at low E_T shows that most $\mathbf{J}'$ and $\mathbf{l}'$ are produced with angles in the 140°–170° range, thus pointing towards an essentially antiparallel character of $\mathbf{J}'$ with respect to $\mathbf{l}'$ (Ref. 44). As E_T goes up, the angle between $\mathbf{J}'$ and $\mathbf{l}'$ shifts progressively down to 90° (Fig. 12), corresponding to an almost symmetric distribution of $\mathbf{J}'$ with respect to $\mathbf{l}'$, thus implying a loss of orien-
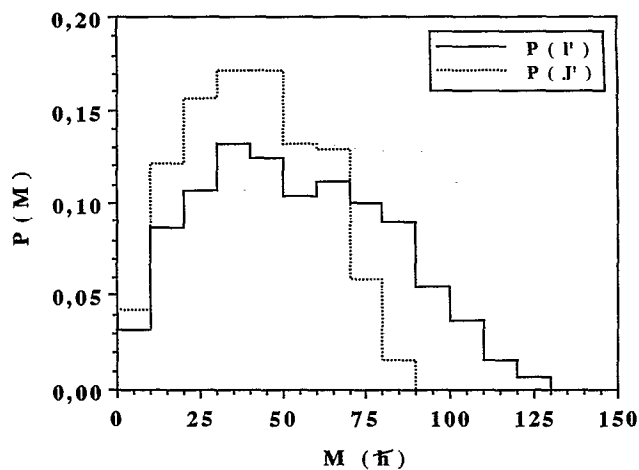

FIG. 11. Distribution of the moduli of the final orbital (l') and rotational (J') angular momenta of products of reaction (1) with $v=0$, $J=7$; $E_T=0.5$ eV.

tation. This fact is probably linked to the progressive change in the scattering mechanism from a markedly backward towards a more forward character. It seems however clear that the most outstanding feature of this PES in what regards the angular momentum disposal in products is its ability to equidistribute the total angular momentum between orbital and rotational angular momenta of products (cf. Table II). A more detailed analysis of the vector properties on this surface is in progress and will be reported in the near future.

IV. CONCLUSIONS

Extensive QCT calculations have been performed for the $N(^4S_u)+NO(X\,^2\Pi)\rightarrow N_2(X\,^1\Sigma_g^+)+O(^3P_g)$ exothermic ($\Delta H^0_{298}=-74.95$ kcal/mol) atmospheric reaction on an accurate analytical Sorbie–Murrell analytical PES built from *ab initio* information for a variety of initial rovibrational levels and relative energy conditions. This process
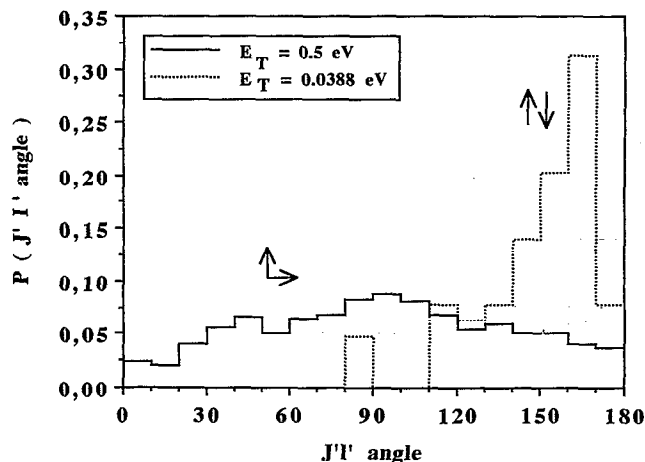

FIG. 12. Distribution of the angle between the final rotational (J') and orbital (l') angular momenta of products of reaction (1) with $v=0$, $J=7$; $E_T=0.0388$ and 0.5 eV.

has been shown to evolve through a direct mechanism implying repulsive energy release. Vibrational excitation of reactants showed a moderate effect on increasing reaction cross section, in full agreement with the early barrier and direct mechanism proposed. Rotational excitation of reactants effectively inhibited reactivity at low E_T, leading to strictly zero reaction cross sections for the higher rotational state of reactants studied at $E_T = 0.0388$ eV. This behavior has been justified in terms of the orientation effect not being effectively compensated for by the energy effect on this repulsive surface.

QCT rate constants at 300, 500, and 700 K are $(1.0 \pm 0.2) \times 10^{13}$, $(1.9 \pm 0.2) \times 10^{13}$, and $(2.1 \pm 0.2) \times 10^{13}$ cm^3/mol s, respectively, quite close to experimental values of $(1.6 \pm 0.3) \times 10^{13}$ (Ref. 13), $(2.3 \pm 0.9) \times 10^{13}$ (Ref. 6), and $(2.9 \pm 1.0) \times 10^{13}$ cm^3/mol s (Ref. 6).

The energy disposal in products has proved to yield translational excitation for all relative energies calculated, with the fraction of available energy going to vibration of products ($\langle f'_v \rangle$) fluctuating slightly over the whole energy range. The QCT value for $v=0$, $J=7$, and $E_T=0.0388$ eV (0.26) is in good agreement with the experimental value at 300 K (0.25–0.28) (Refs. 15 and 16). The observed energy distribution has been accounted for using the proposed mechanism for reaction (1) as well as some simple considerations on the structure of the PES used. A surprisal analysis of the vibrational energy partitioning has revealed the existence of strong constraints at low collision energies, while the statistical distribution was approached at higher E_T. The related translational and rovibrational prior distributions are, respectively, cooler and hotter than the QCT ones even at relatively high E_T. Their mutually compensating effect may account for the statistic-resembling vibrational distribution observed at moderately high energies.

The polar differential cross section indicated a strong backward character at low E_T, unaffected by rotation and vibration of reactants, slowly approaching more forward distributions when larger E_T were used. The angular momentum disposal analysis carried out using the Λ and Λ' macroscopic indicators showed that products were originated with comparable amounts of rotational and orbital angular momenta, thus outlining the role played by the PES in favoring angular momentum equidistribution in products. At low relative energies l' and J' appeared highly antiparallel indicating a strong vector correlation, while on augmentation of E_T, the orientation effect between l' and J' disappeared slowly giving rise to a symmetrical distribution around 90°, in good agreement with the change in the character of the reaction mechanism at moderately high relative energies.

ACKNOWLEDGMENTS

[1] M. Kh. Karapet'yants and M. L. Karapet'yants, *Thermodynamic Constants of Inorganic and Organic Compounds* (Ann Arbor–Humphrey Science, Ann Arbor, MI, 1970).

[2] H. I. Schiff, Ann. Geophys. **20**, 115 (1964).

[3] J. Heicklen and N. Cohen, Adv. Photochem. **5**, 157 (1968).

[4] G. B. Kistiakowsky and G. G. Volpi, J. Chem. Phys. **27**, 1141 (1957).

[5] L. F. Phillips and H. I. Schiff, J. Chem. Phys. **36**, 1509 (1962).

[6] M. A. A. Clyne and I. S. McDermid, J. Chem. Soc. Faraday Trans. **71**, 2189 (1975).

[7] J. H. Lee, J. V. Michael, W. A. Payne, and L. J. Stief, J. Chem. Phys. **69**, 3069 (1978).

[8] M. A. A. Clyne and B. A. Thrush, Proc. R. Soc. London Ser. A **261**, 259 (1961).

[9] J. T. Herron, J. Chem. Phys. **161**, 35 (1978).

[10] Y. Takezaki and S. Mori, Bull. Inst. Chem. Res. Kyoto **45**, 388 (1967).

[11] C. L. Lin, D. A. Parker, and F. Kaufman, J. Chem. Phys. **53**, 3896 (1970).

[12] J. V. Michael and K. P. Lim D. J. Chem. Phys. **97**, 3228 (1992).

[13] D. L. Baulch, D. D. Drysdale and D. G. Haine, *Evaluated Kinetic Data for High Temperature Reactions* (Butterworths, London 1973), Vol. 2.

[14] S. P. Walch and R. L. Jaffe, J. Chem. Phys. **86**, 6946 (1987).

[15] J. E. Morgan, L. F. Phillips, and H. I. Schiff, Discuss. Faraday Soc. **33**, 118 (1962).

[16] G. Black, R. L. Sharpless, and T. G. Slanger, J. Chem. Phys. **58**, 4792 (1973).

[17] M. Gilibert, A. Aguilar, M. González F. Mota, and R. Sayós, J. Chem. Phys. **97**, 5542 (1992).

[18] S. P. Walch and R. L. Jaffe, AIP document No. PAPS JCPSA-86-6946-10.

[19] R. Sayós, A. Aguilar, M. Gilibert, and M. González, J. Chem. Soc. Faraday Trans. (in press).

[20] J. N. L. Connor, J. C. Whitehead, and W. Jakubetz, J. Chem. Soc., Faraday Trans. 2 **83**, 1703 (1987).

[21] M. Gilibert, M. González, and R. Sayós (unpublished work).

[22] D. G. Hopper, Program No. 248, QCPE, Indiana State University, Bloomington, IN, 1974.

[23] M. González and R. Sayós, Chem. Phys. Lett. **164**, 643 (1989).

[24] M. González, A. Aguilar, and R. Sayós, Chem. Phys. **132**, 137 (1989).

[25] R. Sayós, M. González, and A. Aguilar, Chem. Phys. **141**, 402 (1990).

[26] I. W. M. Smith, *Kinetics and Dynamics of Elementary Gas Reactions* (Butterworths, London, 1980).

[27] J. C. Polanyi, Acc. Chem. Res. **5**, 161 (1972).

[28] R. D. Levine and R. B. Bernstein, *Molecular Reaction Dynamics and Chemical Reactivity* (Oxford University, New York, 1979).

[29] I. W. M. Smith, Chem. Soc. Rev. **14**, 141 (1985).

[30] I. Schechter and R. D. Levine, J. Phys. Chem. **93**, 7973 (1989).

[31] N. Sathyamurty, Chem. Rev. **83**, 601 (1983).

[32] A. Persky and M. Broida, J. Chem. Phys. **81**, 4352 (1984).

[33] A. Persky and H. Kornweitz, Chem. Phys. **130**, 129 (1989).

[34] J. A. Harrison, L. J. Isacson, and H. R. Mayne, J. Chem. Phys. **91**, 6906 (1989).

[35] H. Loesch, Chem. Phys. **112**, 85 (1987).

[36] R. Sayós, M. González, and A. Aguilar, Chem. Phys. **98**, 409 (1985).

[37] J. T. Muckerman, J. Chem. Phys. **54**, 1155 (1971).

[38] J. T. Muckerman, J. Chem. Phys. **56**, 2997 (1972).

[39] R. N. Porter, L. M. Raff, and W. H. Miller, J. Chem. Phys. **63**, 2214 (1975).

[40] R. B. Bernstein and R. D. Levine, J. Chem. Phys. **57**, 434 (1972).

[41] A. Ben-Shaul, R. D. Levine, and R. B. Bernstein, J. Chem. Phys. **57**, 5427 (1972).

[42] D. G. Truhlar and J. T. Muckerman, in *Atom Molecule Collision Theory*, edited by R. B. Bernstein (Plenum, New York, 1979).

[43] D. A. Case and D. R. Herschbach, J. Chem. Phys. **64**, 4212 (1976).

[44] S. K. Kim and D. R. Herschbach, Discuss. Chem. Soc. **84**, 159 (1987).

[45] J. M. Alvariño and A. Laganà, J. Chem. Phys. **95**, 998 (1991).

[46] J. M. Alvariño and A. Laganà, Chem. Phys. Lett. **168**, 448 (1990).